Research Article

Cancer Immunology Research

Radiotherapy and CTLA-4 Blockade Shape the TCR Repertoire of Tumor-Infiltrating T Cells

Nils-Petter Rudqvist[1], Karsten A. Pilones[1], Claire Lhuillier[1], Erik Wennerberg[1], John-William Sidhom[2], Ryan O. Emerson[3], Harlan S. Robins[3,4], Jonathan Schneck[2], Silvia C. Formenti[1], and Sandra Demaria[1,5]

Abstract

Immune checkpoint inhibitors activate T cells to reject tumors. Unique tumor mutations are key T-cell targets, but a comprehensive understanding of the nature of a successful antitumor T-cell response is lacking. To investigate the T-cell receptor (TCR) repertoire associated with treatment success versus failure, we used a well-characterized mouse carcinoma that is rejected by CD8 T cells in mice treated with radiotherapy (RT) and anti–CTLA-4 in combination, but not as monotherapy, and comprehensively analyzed tumor-infiltrating lymphocytes (TILs) by high-throughput sequencing of the *TCRB* CDR3 region. The combined treatment increased TIL density and CD8/CD4 ratio. Assessment of the frequency of T-cell clones indicated that anti–CTLA-4 resulted in fewer clones and a more oligoclonal repertoire compared with untreated tumors. In contrast, RT increased the CD8/CD4 ratio and broadened the TCR repertoire, and when used in combination with anti–CTLA-4, these selected T-cell clones proliferated. Hierarchical clustering of CDR3 sequences showed a treatment-specific clustering of TCRs that were shared by different mice. Abundant clonotypes were commonly shared between animals and yet treatment-specific. Analysis of amino-acid sequence similarities revealed a significant increase in the number and richness of dominant CDR3 motifs in tumors treated with RT + anti–CTLA-4 compared with control. The repertoire of TCRs reactive with a single tumor antigen recognized by $CD8^+$ T cells was heterogeneous but highly clonal, irrespective of treatment. Overall, data support a model whereby a diverse TCR repertoire is required to achieve tumor rejection and may underlie the synergy between RT and CTLA-4 blockade. *Cancer Immunol Res; 6(2); 139–50.* ©*2017 AACR.*

Introduction

Immunotherapy that targets immune checkpoints CTLA-4 and PD-1 provides a powerful treatment for many tumors (1). In melanoma patients treated with a blocking monoclonal antibody (mAb) to CTLA-4, neoantigen burden is associated with clinical benefit (2, 3), and a similar association has been reported in lung cancer patients treated with anti–PD-1 (4), suggesting that mutation-generated epitopes are important targets of T-cell responses, which can be unleashed by immune checkpoint blockade (5). On the other hand, shared antigens may be targets of T cell–mediated tumor rejection in tumors with low mutation burden, which are responsive to anti–PD-1 (6). Moreover, patients responding to vaccination with selected tumor antigens showed expansion of T cells specific for multiple tumor antigens in addition to the vaccine, suggesting that mobilization of a broader T-cell repertoire is required for tumor rejection (7).

Accumulated evidence supports the concept that tumor-targeted radiotherapy (RT) can be used to generate an *in situ* tumor vaccine and increase responses to immunotherapy (8). However, the antigenic targets of the T-cell response elicited by RT remain largely undefined. In many preclinical studies, only responses to an exogenous antigen introduced in the cancer cells were monitored (9–12). We have demonstrated that RT elicits CD8 T-cell responses to four epitopes derived from three endogenous antigens that are overexpressed in poorly immunogenic mouse carcinomas if negative immunosuppressive regulators are neutralized (13). Overall, a comprehensive understanding of the nature of T-cell responses elicited by RT in combination with immunotherapy is lacking.

Several immune changes in patients' peripheral blood are associated with response to CTLA-4 blockade, but largely reflect generalized immune activation (14). Next-generation deep sequencing of complementarity-determining region 3 (CDR3) regions in rearranged T-cell receptor β (TCRβ) chain has been used to evaluate the diversity and expansion of T-cell clones in peripheral blood of patients treated with anti–CTLA-4 (15). Observed clonal expansions and losses correlated with immune-related adverse events, suggesting the occurrence of a global turnover of the TCR repertoire (16, 17). However, detailed analysis of T-cell reactivity against a panel of 145 melanoma-associated antigens indicated that a significant

[1]Department of Radiation Oncology, Weill Cornell Medicine, New York, New York. [2]Bloomberg-Kimmel Institute for Cancer Immunotherapy, Johns Hopkins University School of Medicine, Baltimore, Maryland. [3]Adaptive Biotechnologies, Seattle, Washington. [4]Public Health Sciences Division, Fred Hutchinson Cancer Research, Seattle, Washington. [5]Department of Pathology and Laboratory Medicine, Weill Cornell Medicine, New York, New York.

Note: Supplementary data for this article are available at Cancer Immunology Research Online (http://cancerimmunolres.aacrjournals.org/).

N.-P. Rudqvist and K.A. Pilones contributed equally to this article.

Corresponding Author: Sandra Demaria, Weill Cornell Medicine, 1300 York Avenue, Box 169, New York, NY 10065. Phone: 212-746-6068; Fax: 212-746-7815; E-mail: szd3005@med.cornell.edu

doi: 10.1158/2326-6066.CIR-17-0134

number of newly detected tumor-specific T cells were primed by anti–CTLA-4 treatment (18). Thus, data support the ability of anti–CTLA-4 to prime new T-cell responses but also highlight the challenge of detecting such tumor-specific clonal expansions within the peripheral blood. A few studies have analyzed pretreatment and posttreatment tumor biopsies in melanoma patients treated with anti–CTLA-4 and report that an increase in tumor-infiltrating lymphocytes (TILs) or in their activation state is required for tumor rejection (19–21). However, they do not provide information about modulation of TIL specificity by anti–CTLA-4 treatment.

Using as a model for an immunotherapy-refractory tumor the poorly immunogenic 4T1 mouse carcinoma, we previously showed that antitumor immune responses that can reject the primary tumor and distant lung metastases develop only in mice treated with local RT to the primary tumor together anti–CTLA-4, whereas each treatment by itself was ineffective (22). Tumor rejection was mediated by activated CD8 T cells, which infiltrated the irradiated tumor and formed stable MHC class I–dependent interactions with cancer cells (23, 24). Here, we used this well-characterized model to investigate the complexity of the antigen-driven T-cell repertoire associated with successful tumor rejection and compare it to the repertoire elicited by ineffective anti–CTLA-4 treatment. Results show distinct contributions of RT and anti–CTLA-4 to increasing the number and clonality of TILs, with emergence of a unique set of shared TCRs that are treatment-specific. Hierarchical clustering of clones based on CDR3 amino acid (AA) sequence similarity provided additional insights into the diversity of the repertoire, whereas analysis of the repertoire of TCRs reactive with a single tumor antigen demonstrated a heterogeneous but highly clonal response. These data have implication for the evaluation of responses in patients treated with RT and immune checkpoint inhibitors (25–27).

Materials and Methods

Cells and reagents

4T1 cells were obtained from F. Miller, who established this mammary carcinoma cell line (28), and a large stock of low-passage frozen cells was prepared. Cells were authenticated by morphology, growth, and pattern of metastasis *in vivo* and routinely screened for *Mycoplasma* (LookOut Mycoplasma PCR Detection kit, Sigma-Aldrich). Before injection into the mice, cells are routinely cultured for less than a week. Anti-mouse CTLA-4 (mAb clone 9H10, Cat # BE0131) or Syrian hamster IgG isotype control (Cat # BE0087) mAbs were purchased from BioXCell.

Animals and *in vivo* treatment

Six- to eight-week-old female BALB/c mice were obtained from Taconic (Germantown, NY). All *in vivo* experiments were approved by the Institutional Animal Care and Use Committee. Mice were subcutaneously (s.c.) inoculated with 4T1 cells (5×10^4) and assigned randomly to treatment groups 13 days later when tumor have an average diameter of 5 mm. Tumors were irradiated as previously described (13, 22) using the Small Animal Radiation Research Platform (SARRP Xstrahl Ltd) in two doses of 12 Gy each on 2 consecutive days. Control hamster IgG1 or anti–CTLA-4 was given intraperitoneally (i.p.) at 200 μg/mouse on days 15, 18, and 21 post tumor implantation. Tumors were measured every 2 to 3 days using an analog caliper, and mice were euthanized on day 22 for tumor harvest.

Isolation of CD4 and CD8 T cells

Tumors were bisected, and one half of each tumor was used for DNA extraction, whereas the other half from the 4 animals in each treatment group was pooled, minced into small pieces, and digested with 0.2 mg/mL DNAse and 1.67 Wunsch U/mL Liberase (Roche) using established protocols (24, 29). Cell suspensions were filtered through a 40-μm cell strainer, lysed for red blood cells and incubated with anti-mouse CD16/32 (Fc block) prior to staining. Cells were stained with eFluor450 anti-mouse CD45 Clone 30-F11, APC anti-mouse CD4 Clone RM4-5, and FITC anti-mouse CD8a Clone 53-6.7 (eBioscience). $CD4^+$ and $CD8^+$ T cells were sorted using MoFlo cell sorter (DakoCytomation).

Isolation of AH1-reactive CD8 TILs

R-PE–labeled Pro5 MHC class I pentamers linked to the AH1 peptide (SPSYVYHQF) or the MCMV peptide (YPHFMPTNL) were purchased from ProImmune. Briefly, tumors from control or RT+anti–CTLA4-treated mice were harvested at day 22 ($n = 10$ mice/group) and dissociated as described above. Cell suspensions were subjected to a Percoll gradient centrifugation, and the viable lymphocyte layers of 3 to 4 tumors within each group were pooled together to obtain sufficient material for downstream analysis ($n = 3$ pools/group). 10^6 TILs were preincubated with anti-mouse CD16/32 for 10 minutes at 4°C and then stained with a fixable viability dye, before incubation with AH1/H2-L^d or MCMV/H2-L^d pentamers for 20 minutes at room temperature. After washing, fluorochrome-conjugated antibodies against CD8 (clone KT15, Thermo Fischer), CD45 (clone 30-F11, BD Biosciences), CD19 (clone 1D3, eBioscience), and CD11b (clone M1/70, Biolegend) were added for 20 minutes at 4°C. Cells were washed, fixed, and analyzed on a MACSQuant flow cytometer (Miltenyi). The viability dye and the CD19/CD11b antibodies were used as the "dump" gate.

In a similar experiment, we sorted AH1/H2-L^d-pentamer$^+$CD8 T cells from individual tumors of untreated or RT+α-CTLA4-treated mice ($n = 5$ mice/group) using a BD FACSAria-II (BD Biosciences). DNA was isolated from the sorted cells for TCRB CDR3 sequencing as described below. A small fraction of sorted T cells was analyzed for CD69 (clone H1.2F3, eBioscience) expression using a MACSQuant flow cytometer.

Genomic DNA extraction and TCRB CDR3 sequencing

Total genomic DNA (gDNA) from whole tumors, or from sorted tumor-infiltrating CD4, and CD8 T cells, was extracted using Purelink Genomic DNA Kit (Invitrogen) according to the manufacturer's instructions. For the AH1/H2-L^d-pentamer$^+$CD8 T cells, DNA was isolated using the QIAamp DNA Micro Kit. Amplification and sequencing of TCRB CDR3 regions was performed using the ImmunoSEQ platform at Adaptive Biotechnologies (30). The TCRB CDR3 regions used in the sequencing reads were defined according to the ImMunoGeneTics (IMGT) collaboration and a standard algorithm was used to identify which V, D, and J segments contributed to each TCRB CDR3 sequence (31). Only in-frame TCR rearrangements were included in the analysis. For every sample, a standardized amount of DNA was used to amplify and sequence TCRB CDR3 regions. Several molecular and bioinformatic methods are used to control for PCR bias and ensure that the ImmunoSEQ assay is quantitative (30). For every sample investigated synthetic TCR genes are added and act as controls for bioinformatic normalization of amplification bias for every V&J gene segment in the genome. These synthetic molecules

also permit measuring the number of input genomes, and analysis is not performed only on relative abundance between samples. TCR sequence data are publicly available at https://clients.adaptivebiotech.com/pub/rudqvist-2017-cancerimmunologyresearch (https://doi.org/10.21417/B7H34S).

Statistical and bioinformatic analysis

Multiple *t* test analysis within Prism was used to determine statistically significant difference in tumor volumes among treatment groups.

To determine the clonal characteristics of the TCR repertoire for each sample, clonality was calculated as the productive Shannon entropy normalized using the total number of unique productive rearrangements, and subtracting this result from 1 (32). The normalization ensures that the clonality measurement is robust to differences in sample size and enables assessment of relative degree of clonality between samples. The nonparametric Mann–Whitney *U* test was used to determine statistical difference in clonality (*P* values are two-sided and statistical significance defined as $P < 0.05$). In addition, for each animal, clones were ranked from highest to lowest productive frequency. Then, the group average for each clone rank was calculated and used to determine the frequency and cumulative frequency distributions.

For heatmaps used to determine treatment-related clusters of clones, TCR sequencing data were exported from the TCR Analyzer 3.0. For clones with different TCR CDR3 nucleotide sequence but that after translation correspond to the same AA sequence, the frequencies were added together. The cast function from the reshape2 package in RStudio was used to construct a pivot table (RStudio version 0.99.902; R version 3.3.30; reshape2 version 1.4.1; refs. 33, 34). The frequency data was $\log_{10}$ transformed (clones not detected were given a $\log_{10}$ transformed frequency of 0) and used as input for hierarchical clustering (gplots::heatmap.2, version 3.0.1 in R). In some instances, a frequency threshold was used prior to hierarchical clustering (35). Hierarchical clustering was based on CDR3 AA sequence frequency. Additionally, functions in the tcR package in R (Version: 2.2.1.11; ref. 36) were used to analyze parts of the AH1/H2-L^{d}–pentamer^{+}CD8 repertoire.

For ImmunoMap analysis (37), the software and source code for which can be found at https://github.com/sidhomj/ImmunoMap, sequencing data were filtered for productive sequences. All clones with $\geq$5 reads were included in the analysis. Within MATLAB and using the bioinformatics toolbox, sequence distances were calculated between all unique combinations of sequences by calculating global alignment scores via Needleman–Wunsch (WN) global alignment (PAM10 scoring matrix, gap penalty = 30, gap extension penalty = 8). Sequence distance was determined by the following formula:

$$Score12 = Sequence\ Alignment\ Score\ (Sequence\ 1,\ Sequence\ 2)$$
$$Score11 = Sequence\ Alignment\ Score\ (Sequence\ 1,\ Sequence\ 1)$$
$$Score22 = Sequence\ Alignment\ Score\ (Sequence\ 2,\ Sequence\ 2)$$
$$Sequence\ Distance = \left(1 - \frac{Score12}{Score11}\right)\left(1 - \frac{Score12}{Score22}\right)$$

The distance matrix that was computed was used to create weighted dendrograms, in which clones are clustered according to sequence similarity, and the size of the bubble represents clone abundance. Additionally, hierarchical clustering was performed on the distance matrix to create clusters that we termed dominant motifs. A Dominant motif is defined as a cluster of sequences having a sequence distance below a predetermined threshold (37) and with a cumulative frequency (sum of frequencies of sequences in cluster) $\geq$ 1%.

Comparison of similarity of CDR3β sequences of AH1-specific CD8^{+} T cells isolated from 4T1 tumors and from previously described peptide-vaccinated mice (38, 39) was also performed using ImmunoMap. In this analysis, we included 83 AA sequences with productive frequency >1% from AH1-reactive CD8 T cells sorted from tumors of untreated and treated (RT + anti–CTLA-4) mice and the 37 published CDR3β AA sequences from vaccinated mice. For the 30 sequences described by Buhrman and colleagues (39), we used the frequencies of clones in the 15-AH1 group reported in the paper, while for the 7 sequences described by Jordan and colleagues (38), an arbitrary frequency of 14.3% (100/7) was used.

Results

CD8^{+} T cells clonally expand in tumors after radiation and anti–CTLA-4

4T1 is a poorly immunogenic mouse mammary carcinoma mimicking human triple-negative breast cancer. Within about 1 week after implantation into syngeneic BALB/c mice, 4T1 cells form an aggressive highly metastatic and lymphocyte-poor carcinoma resistant to treatment with anti–CTLA-4. Tumor-targeted RT in combination with anti–CTLA-4, but not alone, elicits immune-mediated rejection of the primary tumor and lung metastases, improving the survival rate of the mice and inducing some cures, an effect that is totally dependent on CD8^{+} T cells (22–24, 40).

To analyze changes in TIL repertoire induced by treatment, tumors from 16 mice were harvested at day 22 after inoculation, when the immune-mediated rejection becomes apparent in mice treated with RT + anti–CTLA-4 (refs. 23, 24; Fig. 1A), and divided into two equal portions. One portion was used for CD4^{+} and CD8^{+} T-cell purification after pooling all tumors from the 4 animals in each treatment group to increase available material. DNA was extracted from each purified T-cell sample and from the total tumor half of each individual mouse, and used to perform *TCRB* CDR3 deep sequencing. A total of 2,195 and 535 CDR3 AA sequences were obtained from sorted CD4 and CD8 TILs, respectively, with minimal overlap between the two compartments (Fig. 1B). For each CDR3 sequence identified in a pool, the frequency within each individual tumor from which the pool was prepared was subsequently calculated. Not all of the TCR sequences present in a given tumor were found within the sorted T cells, possibly due to loss of low frequency clones during the sorting procedure (Supplementary Fig. S1). Nevertheless, analysis of the traceable clones demonstrated an inversion in the CD8/CD4 ratio in treated compared with untreated tumors, most dramatic in the RT + anti–CTLA-4 group where CD8^{+} T cells dominated (Fig. 1C).

These findings are consistent with our prior results that CD8^{+} T cells are markedly increased in 4T1 tumors treated with RT + anti–CTLA-4 (23, 24). The expansion of CD8 T cells significantly correlated with increased clonality (Spearman correlation = 0.8944, $P < 0.0001$, Fig. 1D). Clonality was increased within the CD8^{+} compartment in treated, compared with untreated, animals (Fig. 1E).

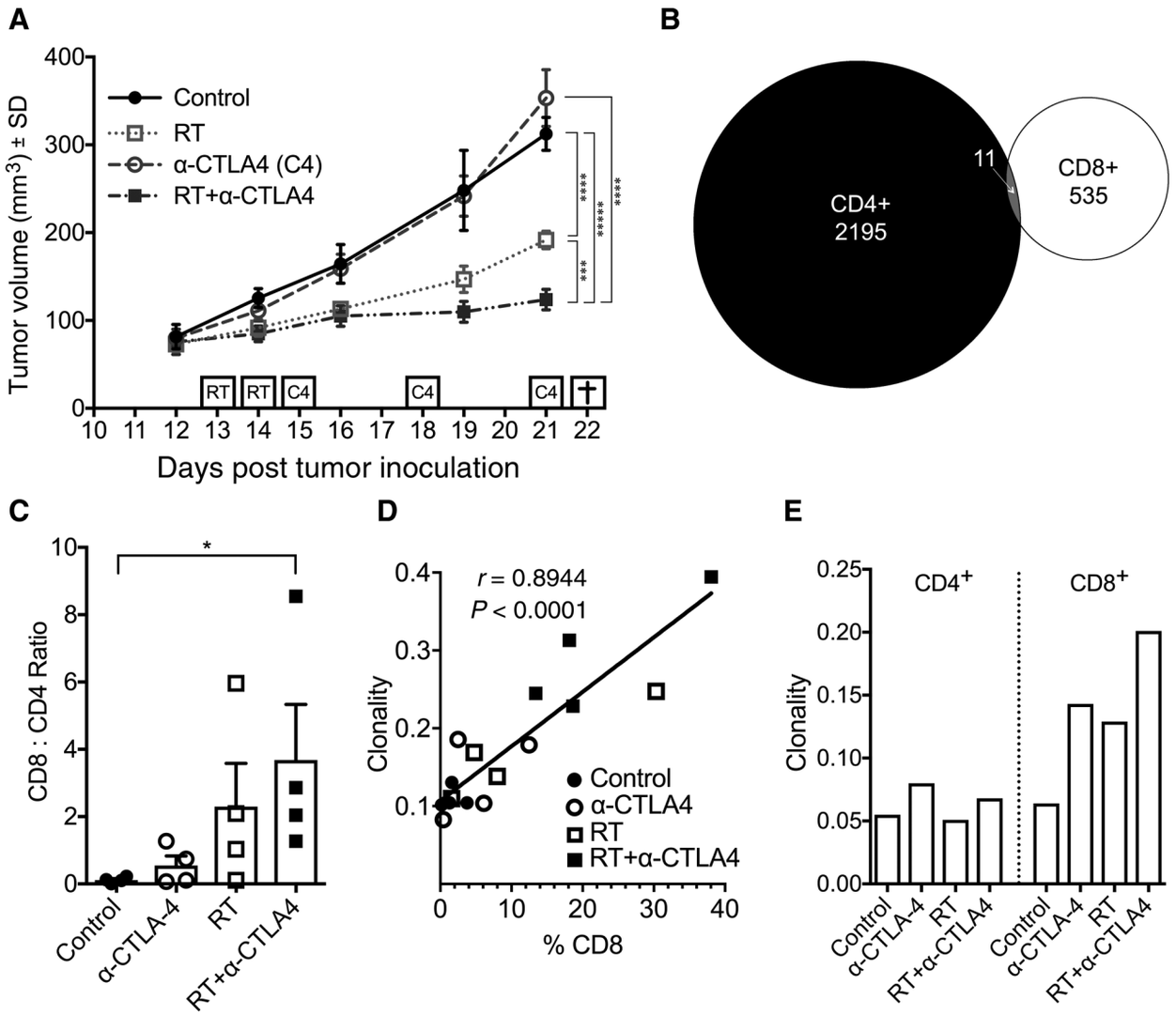

Figure 1.

Increased CD8/CD4 ratio and clonality of intratumoral T cells in 4T1 tumors treated with RT and anti–CTLA-4. **A,** BALB/c mice were injected s.c. with 4T1 cells on day 0. Local RT was given in two fractions of 12 Gy on days 13 and 14. Anti–CTLA-4 or isotype control mAb (C4) was administered i.p. on days 15, 18, and 21 ($n = 4$ mice/group). At day 21, one day before tumors were harvested (†), tumor volume was 312 ± 18.9 mm^3 (control), 353 ± 32.3 (anti–CTLA-4 mAb), 192 ± 10.2 (RT), and 124 ± 11.7 (RT + anti–CTLA-4). Statistical significant differences in tumor volume at day 21 determined with *t* test; ***, $P > 0.0005$; ****, $P > 0.00005$; *****, $P > 0.000005$. **B,** Venn diagram showing minimal overlap between 2195 and 535 CDR3 sequences obtained from sorted $CD4^+$ and $CD8^+$ T cells, respectively, from all 16 tumors. **C,** CDR3 nucleotide sequences of sorted CD4 or CD8 T cells obtained from each treatment group were used to determine the frequencies of these T cells in the tumor samples. Clonal analysis was restricted to those clones that could be unambiguously mapped to either CD4 or CD8 phenotype. Mean proportions from 4 tumors were computed for each treatment group. Statistical significance was determined using the Kruskall–Wallis test (*, $P < 0.01$). **D,** Correlation between sample productive clonality and CD8 composition was plotted for each tumor sample and Spearman correlation computed for each plot. Tumors were split into two equally sized portions. For one portion, DNA was extracted directly from homogenized tumor. For the other portion, DNA was isolated from sorted $CD8^+$ T cells. Clonality was determined from unsorted portion. The $CD8^+$ fraction was calculated as frequency of $CD8^+$ annotated clones in unsorted portion (as determined from the $CD8^+$ sorted cells) divided with total number of clones in the unsorted portion. **E,** Clonality of sorted $CD4^+$ and $CD8^+$ T cells pooled within each treatment group.

Overall, these results support the hypothesis that changes in TIL TCR repertoire induced by RT + anti–CTLA-4 largely reflect clonal expansions of tumor-specific T cells.

Radiation broadens, and anti–CTLA-4 narrows, the TCR repertoire of TIL T cells

To elucidate the effects of each treatment on the TIL TCR repertoire, 4T1 tumor–bearing mice ($n = 5$/group) were treated as shown in Fig. 1A, but the tumor of each animal was used entirely for deep sequencing of *TCRB*. A total of 5,250,077 sequencing reads were obtained, including 22,343 unique productive *TCRB* nucleotide rearrangements (Supplementary Table S1). The clonality (Fig. 2A) was increased in mice treated with anti–CTLA-4. For an in-depth analysis of the clone distribution, clones were ranked from highest to lowest productive frequency for each animal. Then, the group average for

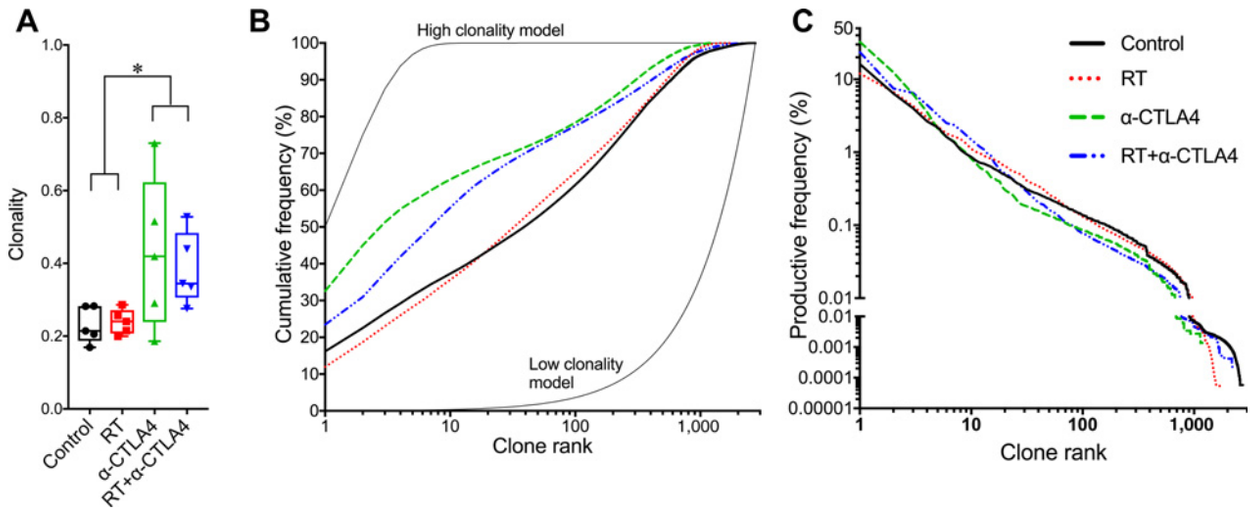

Figure 2.

Clonality and frequency distribution of intratumoral T cells clonotypes. **A,** Clonality was calculated by normalizing productive Shannon entropy using the total number of unique productive rearrangements and subtracting the result from 1 (*, statistical significance: $P < 0.05$, nonparametric Mann–Whitney U test). **B** and **C,** Group average frequency distributions were computed. T-cell clones were ranked according to frequency for each mouse. Then, the group average frequency was calculated for each clone rank. For **B,** two cumulative frequency distributions were also modeled and included in the graph to illustrate a high and low clonality distribution. For the high clonality model, clone with rank n were given a frequency of $50\%/2^{n-1}$. For the low clonality model, all clones shared the frequency of 0.036% (100%/2,751 clones).

each clone rank was calculated. Using these data, the group average frequency distribution of clones was determined (Fig. 2B shows cumulative frequency distribution and 2C the frequency distribution). This analysis revealed that the effect of anti–CTLA-4 was to drive the expansion of a limited number of clones, irrespective of RT; a cumulative frequency of 50% was reached by including only clones 1–3 and 1–7 in the anti–CTLA-4 and RT + anti–CTLA-4 groups, respectively (Fig. 2B). In contrast, in the absence of anti–CTLA-4, a cumulative frequency of 50% was reached when including a much larger number of unique clones (top 33 and 39 clones for the RT and untreated groups, respectively). Additionally, the frequency of clones ranked 11–100 was lower in mice treated with anti–CTLA-4 alone when compared with control (Fig. 2C). In contrast, in RT-treated tumors mid-ranked clones were expanded, resulting in higher frequency of clones 2 to 80 compared with controls (Fig. 2C). In mice treated with RT + anti–CTLA-4 clonal distribution showed features consistent with the effects of both treatments, and clones 1–25 had higher frequency than controls. Thus, the frequency was increased compared with controls for the top-ranked clones, and mid-ranked clones were also expanded. Altogether, these data suggest that anti–CTLA-4 narrows the TCR repertoire in the tumors, whereas radiation broadens it.

New T-cell clones emerge in tumors of mice treated with RT and anti–CTLA-4

To gain further insights into how the TCR repertoire landscape is shaped by RT and anti–CTLA-4, CDR3 AA sequences were analyzed. In all, 19,849 different TCRB CDR3 AA sequences were identified in the tumors of the 20 mice from all four treatment groups. The majority of clones were unique to one individual animal, and only 2,655, 648, and 200 clones were shared between 2, 3, and 4 animals, respectively. Hierarchical clustering of clones present in ≥4 of 20 animals showed several treatment-specific clusters (Fig. 3A). To reduce noise, hierarchical clustering was repeated including only the more abundant clones (productive frequency ≥ 1% in ≥ 1/20 animals). The 137 clones fulfilling this requirement also clustered in a treatment-specific way (Fig. 3B). These clones were rarely (9/137 clones) found in only one individual animal. This suggests that clones present at high level in at least one animal are both commonly shared between animals and treatment-specific and may represent treatment-specific "public" TCRs (41).

Overall, RT + anti–CTLA-4 treatment resulted in clonal expansion of T-cell clones that are not present in untreated tumors, or tumors treated with RT or anti–CTLA-4 monotherapy. Because only the combination of RT and anti–CTLA-4 induces therapeutically effective antitumor responses (22), it is possible that these clonal TCRs recognize tumor antigens that are critical for tumor rejection.

Combination-treated tumors yield increased number and richness of dominant TCRβ CDR3s

The analysis above does not provide information about the sequence similarity of different CDR3 regions. Thus, a newly developed tool, ImmunoMap (37), was used to further interrogate the TCR repertoire. This analytical tool determines similarity between CDR3 AA sequences using the NW algorithm and visualizes the result in a branching tree (dendrogram) with a measurement of frequency shown as a circle in the end of each branch (Fig. 4A). Hierarchical clustering was used to determine CDR3β sequence similarity, with the size of each bubble indicating the frequency of a given clone and the color designating an individual animal carrying the clone. The more similar two clones are (in terms of NW sequence alignment), the closer they will be found in the dendrogram. In the untreated animals, the more abundant clones clustered largely

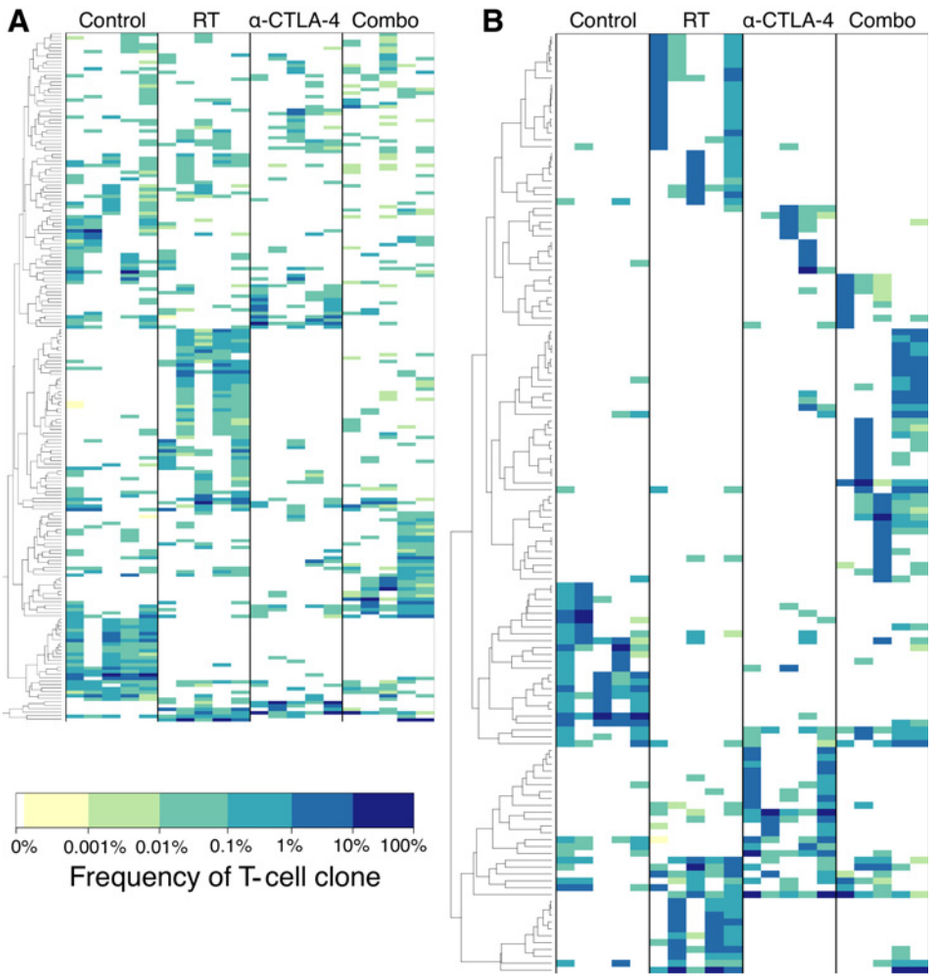

Figure 3.
Hierarchical clustering (HC) of CDR3β sequences shows treatment-related clusters. Each column represents one mouse and each row a clone with unique TCRβ CDR3 AA sequence. Dendrogram represents similarity in clone abundance between animals (i.e., clones clustered together have similar abundance profile among the animals). Colors indicate productive frequency of clone. **A,** HC was performed using clones present in ≥ 4 out of 20 animals in any treatment group. **B,** HC was performed including only clones with ≥1% productive frequency in ≥1/20 animals to reduce noise and focus on the most abundant clones.

in a single branch, indicating that they shared a high degree of similarity (Fig. 4A). Few clones in anti–CTLA-4–treated mice had high frequencies. In contrast, in irradiated tumors the more frequent clones were found in many different branches of the tree, suggesting a broadening of the response, whereby the clones are more divergent in terms of CDR3β region sequence. In tumors of mice treated with the combination of RT and anti–CTLA-4, the response broadened further, with a lower degree of overlap between the individual animals compared with mice that had received only RT. This interpretation is supported by quantification of dominant motifs, i.e., closely related sequences with cumulative frequency >1%, which showed a significant increase only in the latter group (Fig. 4B).

Overall, results of ImmunoMap analysis suggest that RT might expose a new set of antigens leading to priming of T cells that are expanded in the presence of anti–CTLA-4. The data also highlight the variability between individual mice in the combination treatment group.

Longer TCRβ CDR3 regions in TILs from mice treated with radiation and anti–CTLA-4

Hierarchical clustering and ImmunoMap data together indicated a high degree of similarity among the TCRVβ repertoire in the absence of treatment, whereas RT diversified the response. To gain further insights into the effects of treatment on the TCR repertoire of intratumoral T cells we determined the frequency-weighted CDR3 region length distribution for TCR repertoires of the different treatment groups (Fig. 5). Using Prism, a Gaussian fit was calculated for each treatment group, and for all treatment groups combined. The null hypothesis that "one curve fits all treatment groups" was rejected with a P <0.0001. Additionally, CDR3 region length group averages for RT, anti–CTLA-4, and RT + anti–CTLA-4 were all statistically different from that of controls (P: <0.0001, 0.0012, and <0.0001, respectively). RT treatment was primarily associated with an increased mean CDR3 region length without change in the variance of the length distribution (average ± SD: controls, 13.6 ± 1.4 AA; RT, 14.3 ± 1.3 AA). Increased mean CDR3 region length was also seen after anti–CTLA-4 treatment, but the latter primarily reduced the variance of the CDR3 length distribution (14.2 ± 0.69 AA). Combination treatment gave rise to both an increased mean CDR3 length and increased productive frequency of the most common CDR3 region lengths (14.3 ± 0.92 AA). Thus, the T-cell infiltrate in RT-treated tumors is dominated by longer CDR3 regions, suggesting that the increased divergence observed by ImmunoMap analysis may in part reflect decreased representation of germline-encoded Vβ sequences (42).

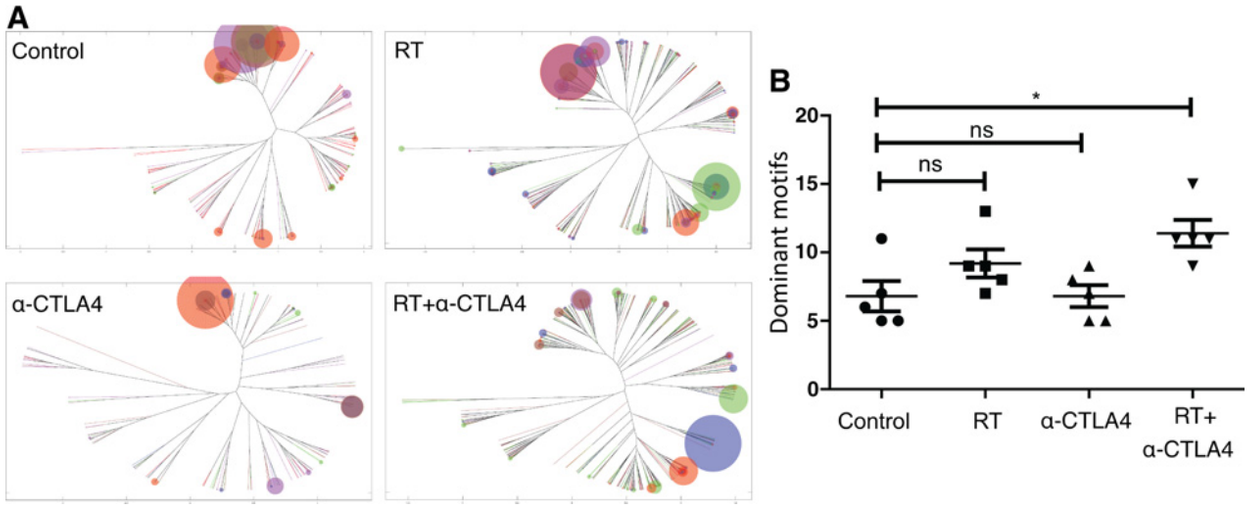

Figure 4.

ImmunoMap metrics of diversity. A distance matrix based on NW similarity score was calculated for all unique TCRβ CDR3 amino acid sequences. Hierarchical clustering was then performed on the distance matrix. **A,** The hierarchical clustering is visualized as weighted unrooted dendrograms. Each color represents one individual animal, and the size of the circles represent frequency of a given clonotype within each animal. **B,** A Dominant motif is defined as a cluster of sequences with a sequence distance below a predetermined threshold and with a cumulative frequency (sum of frequencies of sequences in cluster) $\geq$ 1%. Each dot represents number of dominant motifs for each individual mouse (*, $P < 0.05$, two-tailed unpaired *t* test).

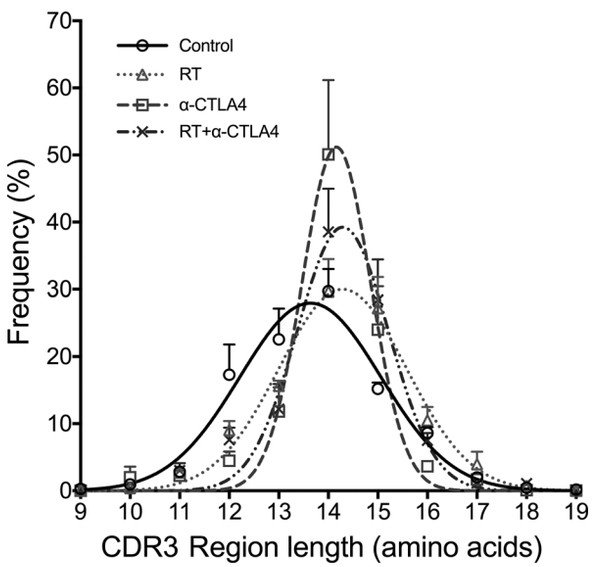

Figure 5.

CDR3 length is different between treatment groups and control. The frequency for each CDR3 region length was calculated for each mouse, and group mean was then calculated for each length. Data points and error bars represent mean + SEM (negative error bars equal positive error bars), $n = 5$. Using Prism, a Gaussian fit was calculated for each treatment group. The null hypothesis, "one curve that fit all treatment groups," was rejected with a $P < 0.0001$. Group average CDR3 region length ± standard deviation: Controls, 13.6 ± 3.4; RT, 14.3 ± 1.3; anti–CTLA-4, 14.2 ± 0.69; RT + anti–CTLA-4, 14.3 ± 0.92. Group average CDR3 length statistically different from controls for RT, anti–CTLA-4, and RT + anti–CTLA-4 (*P*: <0.0001, 0.0012, and <0.0001, respectively).

Expansion and TCR repertoire of CD8 TILs reactive with the dominant AH1 epitope

We have previously shown that $CD8^+$ T-cell responses to the dominant AH1 epitope (SPSYVYHQF), which is derived from the tumor antigen gp70 and presented by H2-L^d, are detected in 4T1 tumor–draining lymph nodes, as measured by IFNγ production, only when mice are treated with RT + anti–CTLA-4, but not in untreated mice or mice treated with RT or anti–CTLA-4 alone, indicating that AH1-specific $CD8^+$ T cells are activated by the combination treatment (40). To evaluate AH1-specific $CD8^+$ TILs, 4T1 tumor–bearing mice were mock-treated or treated with RT + anti–CTLA-4 as in Fig. 1A and tumors harvested for analysis of sorted AH1/H2-L^d pentamer–positive $CD8^+$ T cells. This analysis showed that AH1-reactive $CD8^+$ T cells represented almost a fifth of all $CD8^+$ T cells in untreated tumors. In RT + anti–CTLA-4-treated tumors AH1-reactive T cells were expanded representing about a third of all $CD8^+$ T cells, and were more activated as indicated by higher expression of CD69 (Fig. 6A–C). These results are consistent with our prior findings (24, 40) and indicate that a significant proportion of the $CD8^+$ T cells in untreated and RT + anti–CTLA-4–treated tumors recognize the same shared antigen.

Next, the TCR repertoire of AH1-reactive $CD8^+$ T cells was analyzed by CDR3 sequencing of the sorted AH1-reactive $CD8^+$ T cells, resulting in the identification of 1,933 clones with unique nucleotide rearrangement in 10 animals (195–2,036 unique sequences per animal; Supplementary Table S2). However, within each animal the sorted T cells were highly clonal with the top 5 clones representing 59% to 95% of the repertoire (Fig. 6D). Additionally, within each animal, clones with a frequency of >1% occupied 90% to 97% of the repertoire (Fig. 6E). The 1,933 unique nucleotide CDR3 sequences translated to 1464 unique AA sequences. Comparison of the AA sequences of the top 5 clones within each sorted sample revealed a great degree of diversity within each animal and between different animals

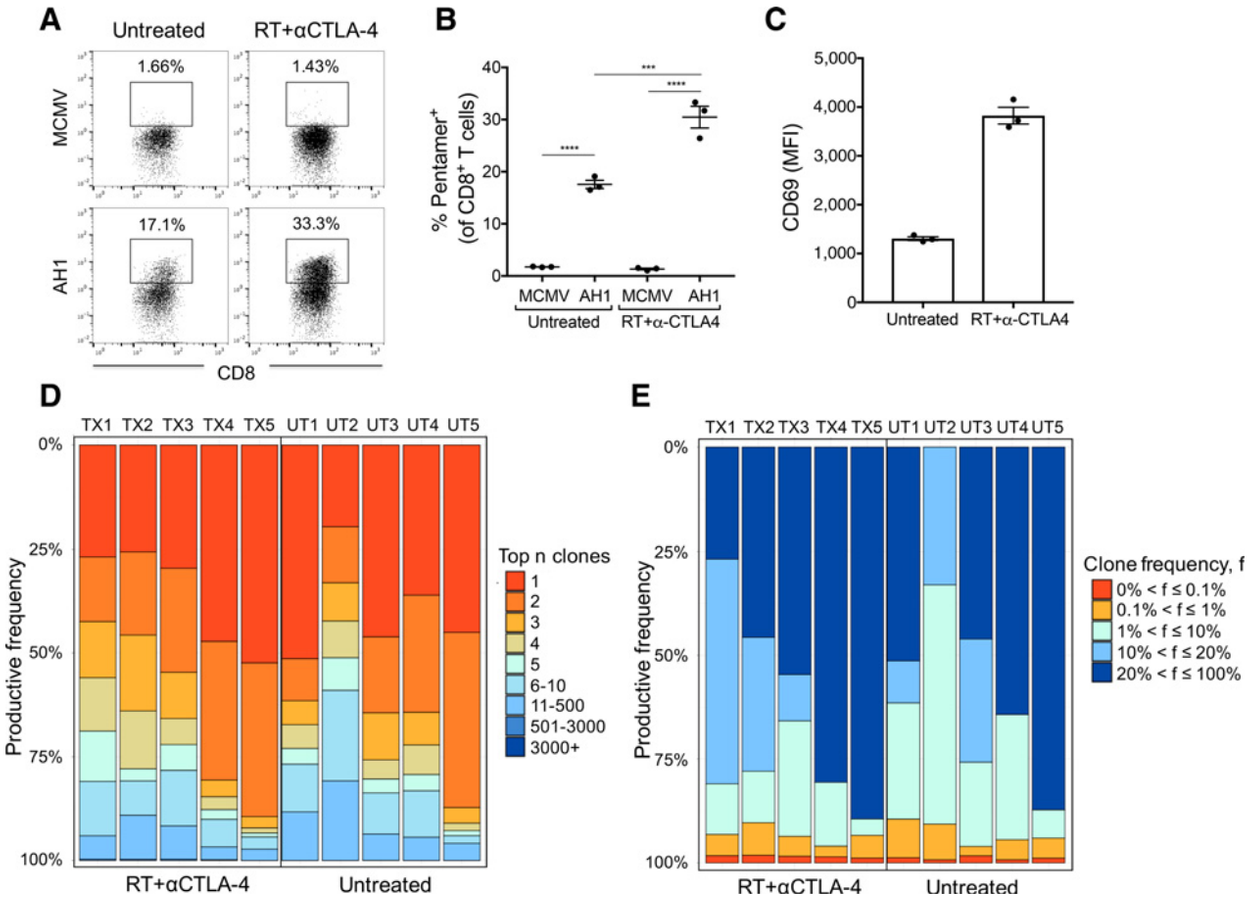

Figure 6.

AH1-specific CD8$^+$ T cells are expended in tumors treated with RT + anti–CTLA4. 4T1 tumors of mice treated as indicated in Fig. 1 were harvested at day 22, dissociated and TILs were isolated using Percoll gradient centrifugation. TILs were then sorted on AH1 specificity using AH1/H2-L^d pentamers. **A,** Representative flow plots of TILs gated on CD45$^+$CD8$^+$dump$^-$ cells. The percentage of cells positive for AH1/H2-L^d pentamer or the control irrelevant MCMV/H2-L^d pentamer is shown. **B,** Percentage of pentamer$^+$ cells among CD8$^+$ TILs. Each dot represents pooled TILs from 3 to 4 individual animals (***, $P < 0.001$; ****, $P < 0.0001$, one-way ANOVA). **C,** CD69 expression of sorted AH1-reactive CD8 T cells from 3 untreated and 3 combination-treated animals (t test $P < 0.0001$). **D,** Visualization of clone frequency occupancy by clone rank (based on nucleotide CDR3 sequence). Each column represents the frequency distribution of all T-cell clones within each individual animal. Color represent clone rank. **E**, Visualization of clone frequency occupancy by clone frequency (based on nucleotide CDR3 sequence). Each column represents the frequency distribution of all clones within one individual animal. Colors designate clone frequencies, and clones are divided into groups based on frequency interval.

(Tables 1 and 2). For example, the sequences of the two top AH1-reactive clones in animal TX4 (treated with RT + anti–CTLA-4) were CASSTDSGNTLYF (47%) and CASSIKTGGFAEQFF (34%). Nevertheless, there were some shared sequences: for example, CASSSRTGGYAEQFF was found in 8 animals. Overall, only 108/1,464 clones were found in more than 1 animal. Importantly, there was no significant difference ($P = 0.11$) in clonality of AH1-reactive T cells between treated and untreated animals (Supplementary Table S2), suggesting that treatment-induced expansion is not focused on a single clone.

The 83 AH1-specific CDR3 AA sequences with >1% frequency were compared with the AA sequences obtained from CD4$^+$ and CD8$^+$ T cells sorted in the experiment shown in Fig. 1. AH1-reactive CDR3 sequences were completely absent from the CD4 compartment, regardless of the treatment group (Supplementary Table S3). In contrast, the AH1-reactive CDR3 sequences represented 2.4% to 15.4% of the CD8 compartment, with the highest representation in RT-treated tumors. The low percentage of AH1-reactive T cells (Fig. 6B) and the low overall frequency of CD8$^+$ T cells in the tumors of untreated and anti–CTLA-4 monotherapy-treated mice (Fig. 1C) may both contribute to the smaller percentage of AH1-reactive CDR3 sequences identified in these groups.

The TCR repertoire of AH1-reactive CD8$^+$ T cells has been characterized in mice vaccinated with the native peptide and altered peptide ligands (38, 39). Of 37 CDR3β AA sequences from vaccinated mice only 3 were found at low frequencies (0.0003%–2%) among the AH1-reactive clones from tumors (Supplementary Table S4). To assess the similarity of the AA sequences isolated from tumors versus vaccinated mice a dendrogram representing the distance matrix of similarity scores was created using ImmunoMap. This analysis revealed that the sequences from vaccinated mice formed a tight cluster, indicating that they share a high degree of similarity (Fig. 7; with CDR3 AA sequences indicated in Supplementary Fig. S2). In contrast,

Table 1. Top five AH1-pentamer$^+$CD8$^+$ sorted T-cell clones in each RT+anti–CTLA-4 treated animal

Mouse	CDR3β region sequence	Frequency (%)[a]	Sequence also found in animals (bold: >5%)[b]						
TX1	CASSAGTTEVFF	26.92							
	CASSAGGSDYTF	15.60							
	CASGATENSDYTF	13.59				UT5			
	CASSIKTGGFAEQFF	12.90	TX2	**TX4**		UT1			
	CASSGGRGEQYF	12.20							
TX2	CASRTGGSYEQYF	25.68							
	CASSSRTGGYAEQFF	20.12	**TX3**	TX4	TX5	**UT2**	UT3	UT4	UT5
	CASSTRTGGYAEQFF	18.74	TX5			UT5			
	CASSIKTGGYAEQFF	14.06	**TX3**			**UT1**	UT3	**UT4**	
	CASSPRDRNTEVFF	2.92				UT1	UT3	**UT5**	
TX3	CASSMKTGGYAEQFF	29.68							
	CASSSRTGGYAEQFF	25.24	**TX2**	TX4	TX5	**UT2**	UT3	UT4	UT5
	CASSIGQGAERLFF	11.20							
	CASSIKTGGYAEQFF	6.31	**TX2**			**UT1**	UT3	**UT4**	
	CASSIPQGRVFF	6.21							
TX4	CASSTDSGNTLYF	47.29							
	CASSIKTGGFAEQFF	33.56	**TX1**	TX2	UT1				
	CALQGANSPLYF	4.05							
	CASSPPGQGYAEQFF	3.10							
	CASSSRTGGYAEQFF	2.38	**TX2**	**TX3**	TX5	**UT2**	UT3	UT4	UT5
TX5	CASSQDNWGGVAETLYF	52.48				UT5			
	CASGEDWGIAETLYF	37.13				UT5			
	CASSIGGASDYTF	2.74							
	CASSLRLGGYAEQFF	1.23	TX2			UT5			
	CASSIKLGGFAEQFF	0.97	TX2						

[a]Productive frequency.
[b]Bold font indicates that the clone was present with a frequency >5% in the animal.

tumor-derived sequences were scattered in multiple branches, without a clear pattern distinguishing clones isolated form treated and untreated mice, which were often found in the same or adjacent branches. Interestingly, there was overall very little similarity between sequences from vaccinated mice and from tumors, but more clones isolated from the untreated than the treated mice were adjacent to the largest cluster from vaccinated mice. Overall, these results suggest that vaccination with a peptide elicits a relatively focused CD8$^+$ T-cell response, whereas presence of a tumor generates a more diverse response, and this diversity is not significantly altered by treatment with RT + anti–CTLA-4.

Discussion

4T1 is a poorly immunogenic carcinoma resistant to anti–CTLA-4 monotherapy but responsive to the combination of

Table 2. Top five AH1-pentamer$^+$CD8$^+$ sorted T-cell clones in each untreated animal

Mouse	CDR3β region sequence	Frequency (%)[a]	Clone also present in animals (bold: >5%)[b]						
UT1	CASSDRGESLYEQYF	51.46							
	CASSRDRGYEQYF	10.16							
	CASSIKTGGYAEQFF	5.80	**TX2**	**TX3**			UT3	**UT4**	
	CTCSGTGSYAEQFF	5.78					UT4		
	CASSRGKYEQYF	3.82							
UT2	CASSSRTGGYAEQFF	19.59	**TX2**	**TX3**	TX4	TX5	UT3	UT4	UT5
	CASSRDRGFEQYF	13.52							
	CASSLTGGAETLYF	9.25							
	CASTTGGREQYF	8.84							
	CASSQVFF	7.88							
UT3	CASSQDGWGGSSYEQYF	46.23							
	CASSDAYYEQYF	18.35							
	CASSRRNSDYTF	11.36							
	CASSQRLGGPTGQLYF	4.62							
	CASSMKLGGYAEQFF	3.38							
UT4	CASGDWGLYEQYF	36.13							
	CASSIKTGGYAEQFF	28.32	**TX2**	**TX3**			**UT1**	UT3	
	CASSPRLGGPTGQLYF	7.88							
	CASSPNRDSQDTQYF	7.15							
	CASSQERTGVAEQFF	3.92							
UT5	CASSPRDRNTEVFF	45.07	TX2				UT1	UT3	
	CASSSRLGGYAEQFF	42.41	TX3				UT1		
	CASSGGTGNSDYTF	3.80							
	CASSSRTGGYAEQFF	1.82	**TX2**	**TX3**	TX4	TX5	**UT2**	UT3	UT4
	CASSQDNWGGVAETLYF	1.22	**TX5**						

[a]Productive frequency.
[b]Bold font indicates that the clone was present with a frequency >5% in the animal.

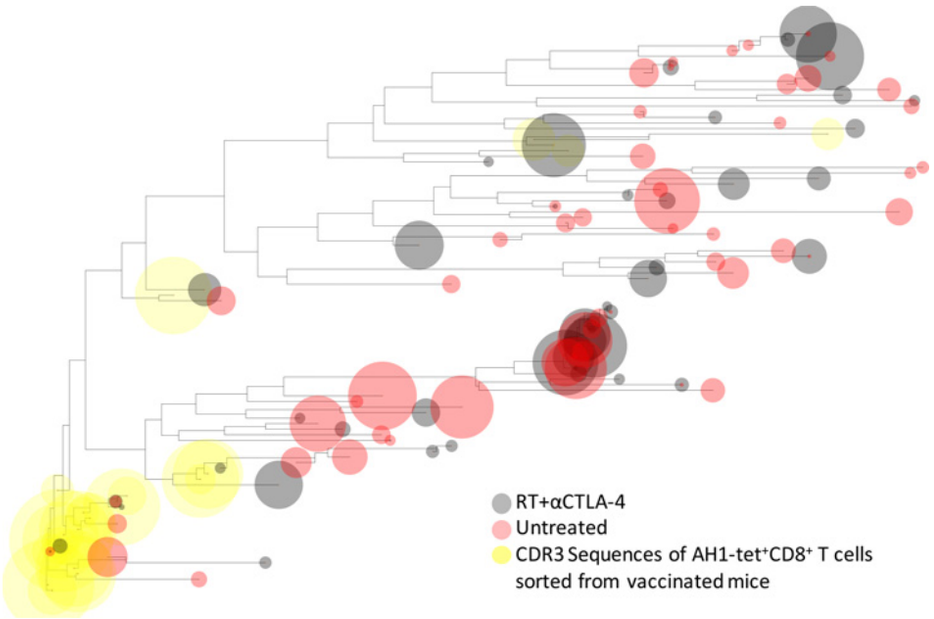

Figure 7.
TCRβ CDR3 amino acid sequence distance among AH1-reactive T cells. A distance matrix based on NW similarity score was calculated between 37 TCRβ CDR3 sequences of T cells sorted from peptide-vaccinated mice (yellow circles) (38, 39) and the 83 AH1-pentamer$^+$CD8 T cells with productive frequency >1% sorted from 4T1 tumors of untreated (red circles) and RT + anti–CTLA-4 treated (gray circles) mice. Hierarchical clustering was performed on the distance matrix and visualized as a frequency weighted dendrogram. Circles size represent frequency of a given clonotype. Supplementary Figure S2 shows the CDR3 amino acids sequences of each clone.

tumor-targeted radiotherapy with anti–CTLA-4, which induces CD8$^+$ T cells capable of rejecting the irradiated tumor and nonirradiated lung metastases (22–24). Here, we show that the population of CD8$^+$ TILs during tumor rejection is largely composed of clonally expanded T cells, about a third of them specific for the AH1 epitope.

Unbiased analysis of the TCRVβ CDR3 regions by deep sequencing revealed treatment-related differences in TIL repertoire. The main effect of anti–CTLA-4 was to drive the expansion of a limited number of clones, whereas RT increased the number of expanded clones (Fig. 2). These results are in agreement with a prior report showing that RT enhanced TCR repertoire diversity in B16 tumors (43). Both top-ranked and mid-ranked clones were expanded in RT + anti–CTLA-4–treated mice. Overall, these observations are consistent with the T cell–intrinsic mechanisms of action of CTLA-4 (44), whereby in the context of low costimulation, blocking CTLA-4 allows expansion of T cells with high-affinity/avidity TCR, whereas in the presence of inflammatory signals elicited by radiation and resulting in increased costimulation, CTLA-4 blockade promotes the proliferation of T cells with TCRs of lower affinity/avidity. Together with the increased cross-presentation of tumor-derived antigens induced by radiation (8), this results in a broadening of the antitumor immune response. It remains to be demonstrated if these complementary effects of RT and CTLA-4 blockade shape a unique repertoire of antitumor T cells that is required for tumor rejection. The observation that the more abundant clones were commonly shared between animals and were treatment-specific (Fig. 3) lends some support to this hypothesis.

Analysis of CDR3 length distribution provided additional evidence of treatment-associated differences in TIL repertoire. Significantly shorter CDR3 sequences were present in tumors of untreated mice compared with other groups. CTLA-4 blockade narrowed the repertoire favoring the expansion of T cells with TCRs containing longer CDR3 sequences, whereas radiation shifted the average CDR3 length upward, but maintained a broad distribution. Although the significance of these changes in the context of tumors is uncertain, Madi and colleagues have also shown that public CDR3 sequences are shorter on average by one AA compared with private sequences, due to lower number of nucleotide insertions in the VD and DJ junctions, and are associated with recognition of self-antigens in mice (41). A shorter CDR3 sequence was also reported in public TCRs isolated from CNS samples of mice with autoimmune encephalomyelitis and was not related to the regulatory phenotype of the T cells (42). Thus, the default TIL repertoire may be largely focused on self-reactive T cells, whereas treatment may expose other types of antigens such as neoantigens.

In this respect, Kretier and colleagues reported the identification of immunogenic mutations in different mouse tumors, including 4T1 and CT26 (45). Of the neoantigens expressed by 4T1 cells, 5 were recognized by CD8$^+$, and 12 by CD4$^+$ T cells. In the CT26 tumor model, vaccination with neoantigens recognized by CD4$^+$ T cells promoted priming of AH1-specific CD8$^+$ T cells by antigenic spread. Thus, it is possible that the broader TCR repertoire in tumors of mice treated with RT + anti–CTLA-4 includes some CD4$^+$ and/or CD8$^+$ T cells reactive with neoantigens, which would similarly contribute to the observed expansion of AH1-reactive CD8$^+$ TILs.

The clonality of AH1-reactive CD8$^+$ TILs was high regardless of treatment, indicating that clonal expansion is a hallmark of antigen-specific T cells. AH1-specific responses may be generated early after tumor inoculation and become suppressed during tumor progression. In fact, AH1-reactive CD8 TILs were present in low numbers and expressed low levels of CD69 in untreated tumors. Their expansion and activation in RT + anti–CTLA-4-treated tumors may be due to a number of factors, including CXCL16-driven recruitment (23). Although they represent about a third of the clonally expanded CD8$^+$ TIL repertoire in treated tumors, their relative contribution to the therapeutic response remains to be ascertained.

Structural analysis of CDR3 AA sequences using a new analytical tool, ImmunoMap, provided additional insights into the nature of TIL TCR repertoire. Clonotypes in irradiated tumors

displayed a significant degree of structural variation compared with nonirradiated tumors. The variability seen among mice receiving the combination treatment could suggest that the same antigen(s) are not targets of T cell–mediated rejection in each mouse. However, the heterogeneity we observed within CDR3 sequences of AH1-reactive CD8 T cells argues against this hypothesis and highlights the limitations of using CDR3 features to predict T-cell antigen specificity.

There are several limitations in our study, including the lack of information on the TCRVα chain CDR3 sequences and their pairing with Vβ chains, and the cross-sectional analysis rather than longitudinal follow-up of individual mice. Nevertheless, our data indicate that treatment with radiation and anti–CTLA-4 leads to dramatic changes in TIL repertoires and suggest that a broader repertoire of tumor-reactive T cells is required for successful tumor rejection. A broad T-cell repertoire targeting multiple antigens has been shown in regressing human tumors responding to vaccination (46, 47), supporting the concept that recruitment of antitumor T cells against a mixture of shared and unique antigens can reach the critical number of T cells required for tumor elimination (7).

Disclosure of Potential Conflicts of Interest

H.S. Robins is cofounder of and has ownership interest in Adaptive Biotechnologies. J. Schneck is a consultant/advisory board member for Neximmune. S. Demaria is a consultant/advisory board member for Eisai, Inc., Lytix Biopharma, Nanobiotix, and AstraZeneca. No potential conflicts of interest were disclosed by the other authors.

Authors' Contributions

Conception and design: K.A. Pilones, S.C. Formenti, S. Demaria
Development of methodology: N.-P. Rudqvist, K.A. Pilones, H.S. Robins, S. Demaria
Acquisition of data (provided animals, acquired and managed patients, provided facilities, etc.): N.-P. Rudqvist, K.A. Pilones, C. Lhuillier, E. Wennerberg, R.O. Emerson, S.C. Formenti
Analysis and interpretation of data (e.g., statistical analysis, biostatistics, computational analysis): N.-P. Rudqvist, K.A. Pilones, C. Lhuillier, J.-W. Sidhom, R.O. Emerson, S. Demaria
Writing, review, and/or revision of the manuscript: N.-P. Rudqvist, K.A. Pilones, J.-W. Sidhom, R.O. Emerson, H.S. Robins, J. Schneck, S.C. Formenti, S. Demaria
Administrative, technical, or material support (i.e., reporting or organizing data, constructing databases): K.A. Pilones
Study supervision: S. Demaria

Acknowledgments

This work was supported by NIH R01CA198533 (to S. Demaria), the Breast Cancer Research Foundation award BCRF-16-054 (to S.C. Formenti and S. Demaria), and the Chemotherapy Foundation (to S. Demaria).

The costs of publication of this article were defrayed in part by the payment of page charges. This article must therefore be hereby marked *advertisement* in accordance with 18 U.S.C. Section 1734 solely to indicate this fact.

Received March 18, 2017; revised September 6, 2017; accepted November 13, 2017; published OnlineFirst November 27, 2017.

References

1. Sharma P, Allison JP. Immune checkpoint targeting in cancer therapy: toward combination strategies with curative potential. Cell 2015;161:205–14.
2. Van Allen EM, Miao D, Schilling B, Shukla SA, Blank C, Zimmer L, et al. Genomic correlates of response to CTLA-4 blockade in metastatic melanoma. Science 2015;350:207–11.
3. Snyder A, Makarov V, Merghoub T, Yuan J, Zaretsky JM, Desrichard A, et al. Genetic basis for clinical response to CTLA-4 blockade in melanoma. N Engl J Med 2014;371:2189–99.
4. Rizvi NA, Hellmann MD, Snyder A, Kvistborg P, Makarov V, Havel JJ, et al. Cancer immunology. Mutational landscape determines sensitivity to PD-1 blockade in non-small cell lung cancer. Science 2015;348:124–8.
5. Schumacher TN, Schreiber RD. Neoantigens in cancer immunotherapy. Science 2015;348:69–74.
6. Motzer RJ, Escudier B, McDermott DF, George S, Hammers HJ, Srinivas S, et al. Nivolumab versus everolimus in advanced renal-cell carcinoma. N Engl J Med 2015;373:1803–13.
7. Coulie PG, Van den Eynde BJ, van der Bruggen P, Boon T. Tumour antigens recognized by T lymphocytes: at the core of cancer immunotherapy. Nat Rev Cancer 2014;14:135–46.
8. Vanpouille-Box C, Pilones KA, Wennerberg E, Formenti SC, Demaria S. In situ vaccination by radiotherapy to improve responses to anti-CTLA-4 treatment. Vaccine 2015;33:7415–22.
9. Lugade AA, Moran JP, Gerber SA, Rose RC, Frelinger JG, Lord EM. Local radiation therapy of B16 melanoma tumors increases the generation of tumor antigen-specific effector cells that traffic to the tumor. J Immunol 2005;174:7516–23.
10. Lee Y, Auh SL, Wang Y, Burnette B, Wang Y, Meng Y, et al. Therapeutic effects of ablative radiation on local tumor require CD8+ T cells: changing strategies for cancer treatment. Blood 2009;114:589–95.
11. Sharabi AB, Nirschl CJ, Kochel CM, Nirschl TR, Francica BJ, Velarde E, et al. Stereotactic radiation therapy augments antigen-specific PD-1-mediated antitumor immune responses via cross-presentation of tumor antigen. Cancer Immunol Res 2015;3:345–55.
12. Schaue D, Ratikan JA, Iwamoto KS, McBride WH. Maximizing tumor immunity with fractionated radiation. Int J Radiat Oncol Biol Phys 2012;83:1306–10.
13. Vanpouille-Box C, Diamond JM, Pilones KA, Zavadil J, Babb JS, Formenti SC, et al. TGFbeta is a master regulator of radiation therapy-induced antitumor immunity. Cancer Res 2015;75:2232–42.
14. Callahan MK, Wolchok JD, Allison JP. Anti-CTLA-4 antibody therapy: immune monitoring during clinical development of a novel immunotherapy. Semin Oncol 2010;37:473–84.
15. Robert L, Tsoi J, Wang X, Emerson R, Homet B, Chodon T, et al. CTLA4 blockade broadens the peripheral T-cell receptor repertoire. Clin Cancer Res 2014;20:2424–32.
16. Cha E, Klinger M, Hou Y, Cummings C, Ribas A, Faham M, et al. Improved survival with T cell clonotype stability after anti-CTLA-4 treatment in cancer patients. Sci Transl Med 2014;6:238ra70.
17. Subudhi SK, Aparicio A, Gao J, Zurita AJ, Araujo JC, Logothetis CJ, et al. Clonal expansion of CD8 T cells in the systemic circulation precedes development of ipilimumab-induced toxicities. Proc Natl Acad Sci USA 2016;113:11919–24.
18. Kvistborg P, Philips D, Kelderman S, Hageman L, Ottensmeier C, Joseph-Pietras D, et al. Anti-CTLA-4 therapy broadens the melanoma-reactive CD8+ T cell response. Sci Transl Med 2014;6:254ra128.
19. Ji R-R, Chasalow SD, Wang L, Hamid O, Schmidt H, Cogswell J, et al. An immune-active tumor microenvironment favors clinical response to ipilimumab. Cancer Immunol Immunother 2012;61:1019–31.
20. Hamid O SH, Nissan A, Ridolfi L, Aamdal S, Hansson J, Guida M, et al. A prospective phase II trial exploring the association between tumor microenvironment biomarkers and clinical activity of ipilimumab in advanced melanoma. J Transl Med 2011;9:204.
21. Chen PL, Roh W, Reuben A, Cooper ZA, Spencer CN, Prieto PA, et al. Analysis of immune signatures in longitudinal tumor samples yields insight into biomarkers of response and mechanisms of resistance to immune checkpoint blockade. Cancer Discov 2016;6:827–37.

22. Demaria S, Kawashima N, Yang AM, Devitt ML, Babb JS, Allison JP, et al. Immune-mediated inhibition of metastases after treatment with local radiation and CTLA-4 blockade in a mouse model of breast cancer. Clin Cancer Res 2005;11:728–34.
23. Matsumura S, Wang B, Kawashima N, Braunstein S, Badura M, Cameron TO, et al. Radiation-induced CXCL16 release by breast cancer cells attracts effector T cells. J Immunol 2008;181:3099–107.
24. Ruocco MG, Pilones KA, Kawashima N, Cammer M, Huang J, Babb JS, et al. Suppressing T cell motility induced by anti-CTLA-4 monotherapy improves antitumor effects. J Clin Invest 2012;122:3718–30.
25. Postow MA, Callahan MK, Barker CA, Yamada Y, Yuan J, Kitano S, et al. Immunologic correlates of the abscopal effect in a patient with melanoma. N Engl J Med 2012;366:925–31.
26. Golden EB, Demaria S, Schiff PB, Chachoua A, Formenti SC. An abscopal response to radiation and ipilimumab in a patient with metastatic non-small cell lung cancer. Cancer Immunol Res 2013;1:365–72.
27. Kang J, Demaria S, Formenti S. Current clinical trials testing the combination of immunotherapy with radiotherapy. J Immunother Cancer 2016;4:51.
28. Aslakson CJ, Miller FR. Selective events in the metastatic process defined by analysis of the sequential dissemination of subpopulations of a mouse mammary tumor. Cancer Res 1992;52:1399–405.
29. Pilones KA, Kawashima N, Yang AM, Babb JS, Formenti SC, Demaria S. Invariant natural killer T cells regulate breast cancer response to radiation and CTLA-4 blockade. Clin Cancer Res 2009;15:597–606.
30. Carlson CS, Emerson RO, Sherwood AM, Desmarais C, Chung MW, Parsons JM, et al. Using synthetic templates to design an unbiased multiplex PCR assay. Nat Commun 2013;4:2680.
31. Monod MY, Giudicelli V, Chaume D, Lefranc MP. IMGT/Junction Analysis: the first tool for the analysis of the immunoglobulin and T cell receptor complex V-J and V-D-J JUNCTIONs. Bioinformatics 2004;20:379–85.
32. Sherwood AM, Emerson RO, Scherer D, Habermann N, Buck K, Staffa J, et al. Tumor-infiltrating lymphocytes in colorectal tumors display a diversity of T cell receptor sequences that differ from the T cells in adjacent mucosal tissue. Cancer Immunol Immunother 2013;62:1453–61.
33. Team RC. R: A language and environment for statistical computing. Vienna: R Foundation for Statistical Computing; 2014. 2016.
34. Wickham H. Reshaping data with the reshape package. J Stat Softw 2007;21:1–20.
35. Warnes GR, Bolker B, Bonebakker L, Gentleman R, Huber W, Liaw A, et al. gplots: Various R programming tools for plotting data. R package version. 2009;2.
36. Nazarov VI, Pogorelyy MV, Komech EA, Zvyagin IV, Bolotin DA, Shugay M, et al. tcR: an R package for T cell receptor repertoire advanced data analysis. BMC Bioinformatics 2015;16:175.
37. Sidhom J-W, Bessell CA, Havel JJ, Kosmides A, Chan TA, Schneck JP. ImmunoMap: a novel bioinformatics tool for T-cell repertoire analysis. Cancer Immunol Res 2018;6:151–62.
38. Jordan KR, Buhrman JD, Sprague J, Moore BL, Gao D, Kappler JW, et al. TCR hypervariable regions expressed by T cells that respond to effective tumor vaccines. Cancer Immunol Immunother 2012;61:1627–38.
39. Buhrman JD, Jordan KR, U'Ren L, Sprague J, Kemmler CB, Slansky JE. Augmenting antitumor T-cell responses to mimotope vaccination by boosting with native tumor antigens. Cancer Res 2013;73:74–85.
40. Pilones KA, Aryankalayil J, Babb JS, Demaria S. Invariant natural killer T cells regulate anti-tumor immunity by controlling the population of dendritic cells in tumor and draining lymph nodes. J Immunother Cancer 2014;2:37.
41. Madi A, Shifrut E, Reich-Zeliger S, Gal H, Best K, Ndifon W, et al. T-cell receptor repertoires share a restricted set of public and abundant CDR3 sequences that are associated with self-related immunity. Genome Res 2014;24:1603–12.
42. Zhao Y, Nguyen P, Ma J, Wu T, Jones LL, Pei D, et al. Preferential use of public TCR during autoimmune encephalomyelitis. J Immunol 2016;196:4905–14.
43. Twyman-Saint Victor C, Rech AJ, Maity A, Rengan R, Pauken KE, Stelekati E, et al. Radiation and dual checkpoint blockade activate non-redundant immune mechanisms in cancer. Nature 2015;520:373–7.
44. Peggs KS, Quezada SA, Allison JP. Cell intrinsic mechanisms of T-cell inhibition and application to cancer therapy. Immunol Rev 2008;224:141–65.
45. Kreiter S, Vormehr M, van de Roemer N, Diken M, Löwer M, Diekmann J, et al. Mutant MHC class II epitopes drive therapeutic immune responses to cancer. Nature 2015;520:692–6.
46. Lurquin C, Lethe B, De Plaen E, Corbiere V, Theate I, van Baren N, et al. Contrasting frequencies of antitumor and anti-vaccine T cells in metastases of a melanoma patient vaccinated with a MAGE tumor antigen. J Exp Med 2005;201:249–57.
47. Carrasco J, Van Pel A, Neyns B, Lethe B, Brasseur F, Renkvist N, et al. Vaccination of a melanoma patient with mature dendritic cells pulsed with MAGE-3 peptides triggers the activity of nonvaccine anti-tumor cells. J Immunol 2008;180:3585–93.